Available online at www.sciencedirect.com

ScienceDirect

Journal of the European Ceramic Society 35 (2015) 2041–2049

www.elsevier.com/locate/jeurceramsoc

$LaNiO_3$ seed layer induced enhancement of piezoelectric properties in (1 0 0)-oriented $(1-x)$BZT–xBCT thin films

W.L. Li [a,b,*], T.D. Zhang [a], D. Xu [a], Y.F. Hou [a], W.P. Cao [a], W.D. Fei [a,c]

[a] *School of Materials Science and Engineering, Harbin Institute of Technology, Harbin 150001, PR China*
[b] *National Key Laboratory of Science and Technology on Precision Heat Processing of Metals, Harbin Institute of Technology, Harbin 150001, PR China*
[c] *State Key Laboratory of Advanced Welding and Joining, Harbin Institute of Technology, Harbin 150001, PR China*

Received 20 October 2014; received in revised form 14 January 2015; accepted 14 January 2015
Available online 28 January 2015

Abstract

The (1 0 0)-oriented ferroelectric lead-free $(1-x)Ba(Zr_{0.2}Ti_{0.8})O_3$–$xBa_{0.7}Ca_{0.3}TiO_3$ (BZT–xBCT) thin films were grown on Pt(1 1 1)/Ti/SiO_2/Si substrates by sol–gel method, and $LaNiO_3$ (LNO) seed layer was introduced between the film and the substrate. The insertion of LNO seed layer greatly improves the quality of the films and enhances the piezoelectric properties. Both of the compositions, $x = 0.50$ and $x = 0.55$, have relatively higher d_{33} values around MPB, and the piezoelectric coefficient is 113.6 pm/V and 131.5 pm/V, respectively. The result of $\varepsilon_r \sim T$ spectrum implies that dielectric permittivity has a weak temperature dependence from 30 °C to 150 °C.

Keywords: BZT–BCT film; $LaNiO_3$ seed layer; Orientation; Piezoelectric properties

1. Introduction

The researches on high-performance lead-free piezoelectric materials,[1–3] e.g. $BaZr_xTi_{1-x}O_3$ (BZT), $Na_xK_{1-x}NbO_3$ (KNN), $Bi_xNa_{1-x}TiO_3$ (NBT), etc., have attracted much attention because of the environmental pollution caused by PbO in lead-based piezoelectric, like $PbZr_xTi_{1-x}O_3$ (PZT).[4,5] In particular, it was reported that $0.5Ba(Zr_{0.2}Ti_{0.8})O_3$–$0.5(Ba_{0.7}Ca_{0.3})TiO_3$ ceramic shows a surprisingly high piezoelectric coefficient of $d_{33} \sim 620$ pC/N at morphotropic phase boundary (MPB).[6] This exciting d_{33} value inspires many researchers to study BZT–BCT thin films. However, it is very difficult to obtain well-crystallized and dense BZT–BCT thin film without crack. In 2011, Kang et al.[7] firstly prepared dense BZT–BCT thin film with random orientation by chemical solutions method, in spite of its relatively small piezoelectric coefficient d_{33} of 71.7 pm/V. At the same year, Piorra et al.[8] attained the (1 1 1)-oriented 0.5BZT–0.5BCT thin film with a piezoelectric coefficient of 80 pm/V via pulsed laser deposition method, and a high effective piezoelectric coefficient d_{33} of 100 ± 5 pm/V was reported by Luo et al.[9]

In the research of the BZT–BCT films, the improvement of the film's quality, which can be realized by modifying preparation methods, and the enhancement of piezoelectric properties of BZT–BCT films become the most important aspects. Unfortunately, the reported d_{33} values of BZT–BCT films are smaller compared with $d_{33} \approx 100$–250 pm/V of PZT thin films.[10–12] Thus, how to obtain well-crystallized BZT–BCT films with a high d_{33} value becomes a crucial point. In addition, the so-called MPB region, in which thin films or bulk ceramics will exhibit excellent piezoelectric, dielectric, and ferroelectric properties, may be quite different in the film and bulk materials even if they are with the same composition because of the residual stress existing in films. Therefore, it is worth identifying the MPB of BZT–BCT films.

Above all, it is very necessary to investigate $(1-x)$BZT–xBCT thin films with high quality and excellent

* Corresponding author at: School of Materials Science and Engineering, Harbin 150001, PR China. Tel.: +86 451 86415894; fax: +86 451 86415894.
E-mail address: wlli@hit.edu.cn (W.L. Li).

http://dx.doi.org/10.1016/j.jeurceramsoc.2015.01.018
0955-2219/

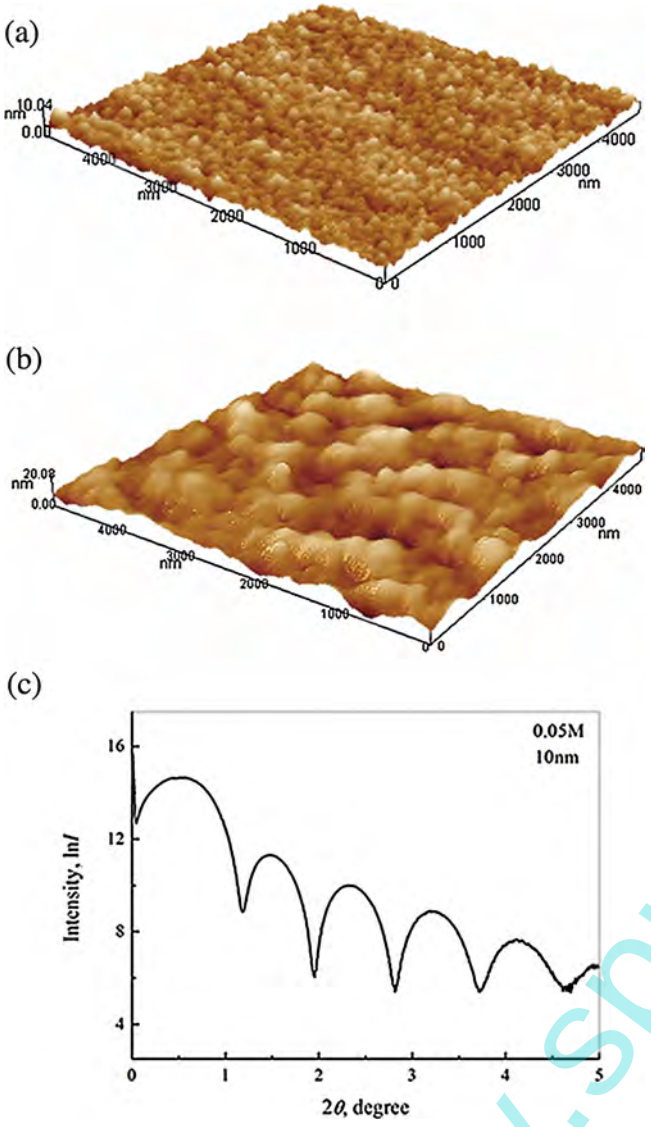

Fig. 1. The three-dimensional image and thickness of the LNO seed layer. (a) AFM image of Pt/Si substrate, (b) AFM image of LNO seed layer, and (c) XRR curve of LNO seed layer.

piezoelectric properties. In this paper, we present a simple but effective way to improve crystallization quality of the film and enhance its piezoelectric properties by inserting LNO seed layer between the film and Pt(1 1 1)/Ti/SiO_2/Si substrates using sol–gel method. The microstruture, ferroelectric polarization hysteresis loops, together with piezoelectric properties of the (1 0 0)-orientated $(1-x)$BZT–xBCT thin films were discussed. At last, the T_m was given according to the experiment of temperature dependence of dielectric permittivity.

2. Experimental procedure

The barium acetate [$Ba(CH_3COO)_2$], calcium acetate [$Ca(CH_3COO)_2$], zirconium *n*-propoxide and titanium isopropoxide were used as raw materials for fabricating BZT–BCT thin films. Acetic acid and 2-methoxyethanol were used as the

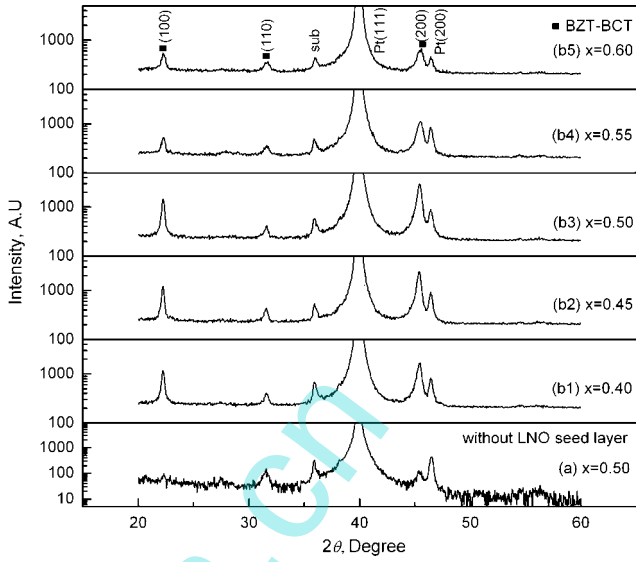

Fig. 2. XRD patterns of $(1-x)$BZT–xBCT thin film. (a) $x = 0.50$ thin film without LNO seed layer, (b) XRD patterns of $(1-x)$BZT–xBCT thin films with LNO seed layer. (b1) $x = 0.40$, (b2) $x = 0.45$, (b3) $x = 0.50$, (b4) $x = 0.55$, and (b5) $x = 0.60$.

solvent. Firstly, [$Ba(CH_3COO)_2$] and [$Ca(CH_3COO)_2$] were dissolved in acetic acid and refluxed at 80 °C for 30 min, and then zirconium *n*-propoxide and titanium isopropoxide were added into the above solution when it cooled down to room temperature. After refluxing for another 30 min, the concentration of the solution was adjusted to 0.35 mol/L by adding 2-methoxyethanol. $LaNiO_3$ (LNO) solution was used for preparing the seed layer. The raw materials were Lanthanum nitrate [$La(NO_3)_3$] and Nickel acetate [$Ni(CH_3COO)_2$]. $La(NO_3)_3$ and $Ni(CH_3COO)_2$ were initially dissolved and refluxed for 30 min in heated 2-methoxyethanol, and the concentration of the solution was adjusted to 0.05 mol/L. The preparation of the precursor solutions was carried out in a glove box in N_2 ambient. After aging the precursor solution for 24 h, LNO seed layer and $(1-x)$BZT–xBCT thin films were deposited on Pt(1 1 1)/Ti/SiO_2/Si substrates through a sol–gel process. Firstly, a thin LNO layer was deposited onto the Pt(1 1 1)/Ti/SiO_2/Si substrate and followed by pyrolysis at 375 °C for 3 min, and then the seed layer was annealed at 750 °C for 30 min. Next, $(1-x)$BZT–xBCT, where x is the molar percent of BCT, thin films were grown on LNO/Pt(1 1 1)/Ti/SiO_2/Si with the spin-coating at 4000 rpm for 15 s. Each spin coated thin film was dried in air at 375 °C for 5 min, and the thickness of the film was adjusted to approximately 200 nm by repeating coating/heating cycle. Finally, the resulting films were heated at 750 °C for 30 min for crystallization.

The crystalline structures of the thin films were analyzed by a Philips X' pert X-ray diffractometer (XRD) with Cu Kα radiation generated at 40 kV and 40 mA. We proposed a universal fiber texture on the basis of ω-scan XRD. During the ω-scan XRD measurement, the diffraction angle $2\theta_{hkl}$ with respect to the diffracting plane ($h\,k\,l$) was fixed and the incidence angle ω of X-ray can be continuously changed from 0 to

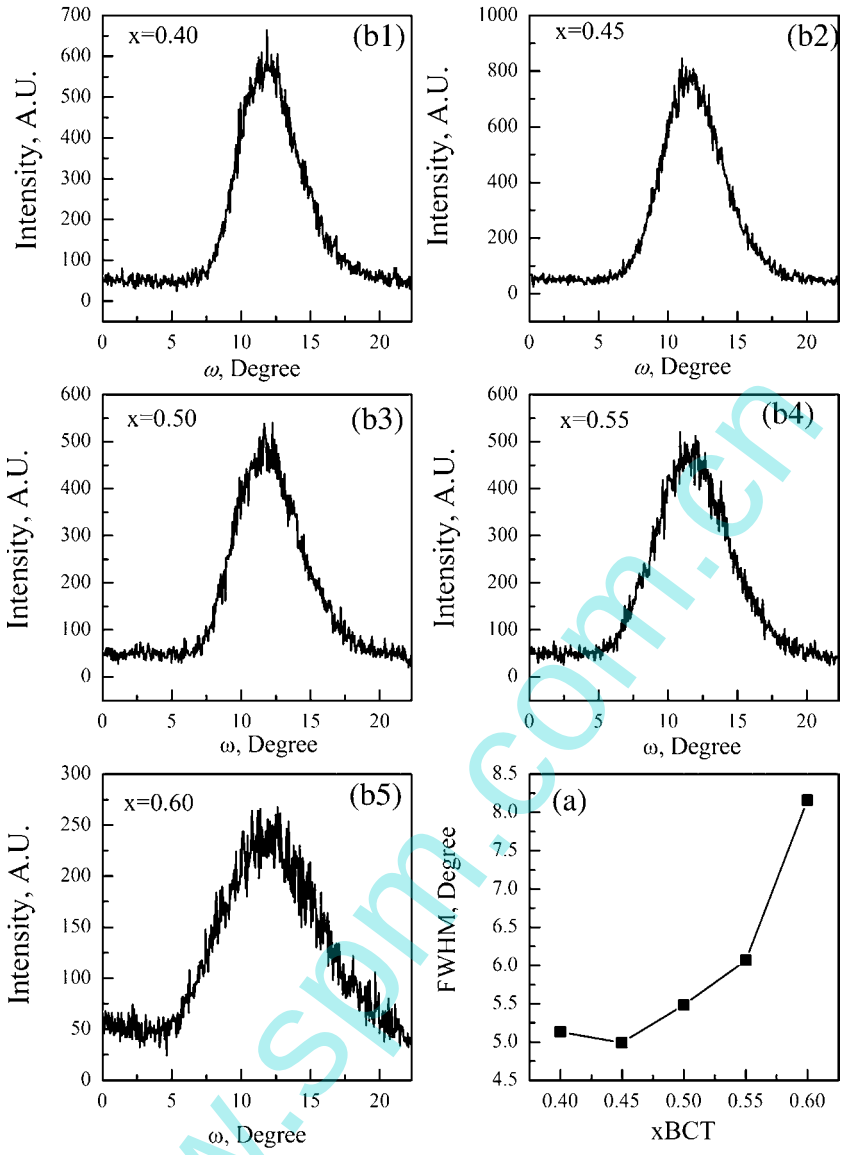

Fig. 3. The XRD ω-scan for the (1 0 0)-textured (1 − x)BZT–xBCT thin films with LNO seed layer. (b1) x = 0.40, (b2) x = 0.45, (b3) x = 0.50, (b4) x = 0.55, and (b5) x = 0.60, (a) FWHM values with x variation.

$2\theta_{hkl}$. The ferroelectric properties were characterized by a Radiant Precision Workstation Ferroelectric Measurement System. The piezoelectric properties were measured with a piezoelectric force microscopy (PFM) in contact mode and the surface morphology of the thin films was observed by atomic force microscopy (AFM) using a commercial setup scanning probe microscope system (CSPM5600 of Benyuan) equipped with a lock-in amplifier (model SR530, Stanford Research Systems, Inc.). The piezoelectric constants of the samples were measured with poled ahead of time. In the poling process, the BZT–xBCT thin films were applied a voltage of 500 kV/cm for 10 min. For measurements of converse piezoelectric coefficients d_{33} in all films, the top platinum electrodes with the same size of 3.14×10^{-4} cm^2 were contacted with conductive tip. The input ac sine wave voltage, amplitude in the range of 0.5–3.5 V and frequency 5 kHz which was chosen far away from resonant frequencies of the cantilever and acquiring the piezoelectric response during each pulse, was applied between the conductive tip and bottom electrode in the thickness direction. The corresponding vertical deflection signal of the cantilever is recorded by lock-in amplifier. By multiplying the deflection signal with the calibration constant of the photodetector sensitivity, the amplitude of the tip vibration was derived. The details and advantages of the PFM method have been described elsewhere.[13] The cross-section micrograph of the thin film was performed by SEM (Helios Nanolab600i). As the top electrode, platinum electrodes with a size of 3.14×10^{-4} cm^2 were deposited by DC magnetron sputtering. Temperature dependence of dielectric properties of the sample was measured at frequencies ranging from 100 Hz to 100 kHz using an Agilent 4294A precision impedance analyzer.

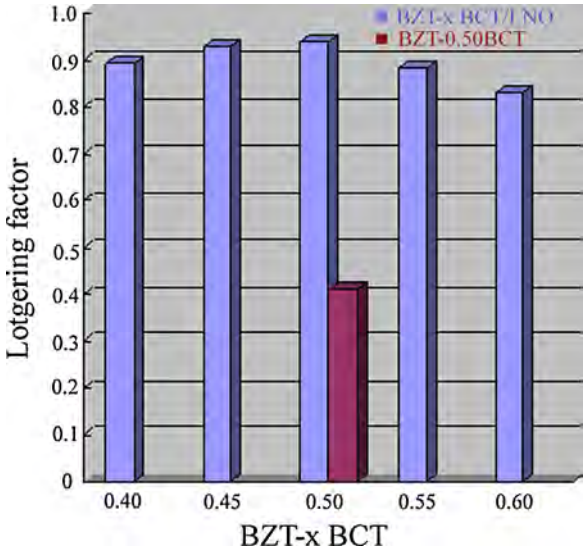

Fig. 4. The Lotgering factor $f(1\,0\,0)$ as a function of xBCT content.

The temperature increased from room temperature (30 °C) to 150 °C by Sigma heating system with the heating rate of 2 °C/min.

3. Results and discussion

The three-dimensional image and thickness of the LNO seed layer were characterized by AFM and X-ray reflectivity (XRR) techniques. As shown in Fig. 1, the Pt(1 1 1)/Ti/SiO_2/Si substrate shows much denser and finer grains, while the grains of the LNO seed layer become much coarser. As shown in Fig. 1(c), a Kissige fluctuation, characterizing the thickness of the film, can be found at low angles. According to the XRR result, the thickness of the LNO seed layer is only about 10 nm, leading to no diffraction peaks of LNO seed layer in the XRD pattern.

The XRD patterns of $(1-x)$BZT–xBCT thin films with different x content on the LNO seed layer are shown in Fig. 2. The XRD diffraction patterns indicate that all the thin films have a pure perovskite structure without any trace of secondary phases. Compared with BZT–0.50BCT thin film without LNO seed layer (see Fig. 2(a)), $(1-x)$BZT–xBCT films with LNO seed layer which hereafter is referred as $(1-x)$BZT–xBCT/LNO, have some degree of (1 0 0) orientation.

To observe the orientation distribution in the $(1-x)$BZT–xBCT/LNO thin films, we performed XRD ω-scan for the thin films.[14,15] As revealed in Fig. 3, all the ω-scan patterns show symmetric Gauss distribution, where the full width at half maximum (FWHM) is less than 8.5°. It suggests that there exists some degree of (1 0 0) orientation in the films. Moreover, with increasing xBCT content, FWHM values become small first, then increase gradually. Usually, a smaller FWHM value means a stronger orientation distribution among the grains with a (1 0 0) orientation. The result indicates that the BZT–0.45BCT/LNO thin film possesses the strongest orientation degree. In order to give a more quantitative estimation of films' orientation, the degree of orientation was evaluated using the Lotgering orientation factor method[16,17] from the intensities of XRD measurement in the range of $20° \leq 2\theta \leq 60°$. As shown in Fig. 4, with the increasing xBCT content, the variation of the Lotgering factor $f(1\,0\,0)$ values was almost consistent with the results of ω-scan. The Lotgering factor $f(1\,0\,0)$ was calculated to be 0.94 and 0.41 for the BZT–0.50BCT/LNO and BZT–0.50BCT film, respectively, indicating the existence of (1 0 0) orientation caused by the insertion of LNO seed layer.

To further support the well-crystallization of $(1-x)$BZT–xBCT/LNO thin film, AFM surface observation was carried out for BCT–0.50BZT thin film, the one with LNO seed layer and the other one without LNO seed layer. As can be seen in Fig. 5, compared with the one without LNO seed layer, BZT–0.50BCT/LNO exhibits a more uniform and denser surface structure with a more homogeneous grain size,

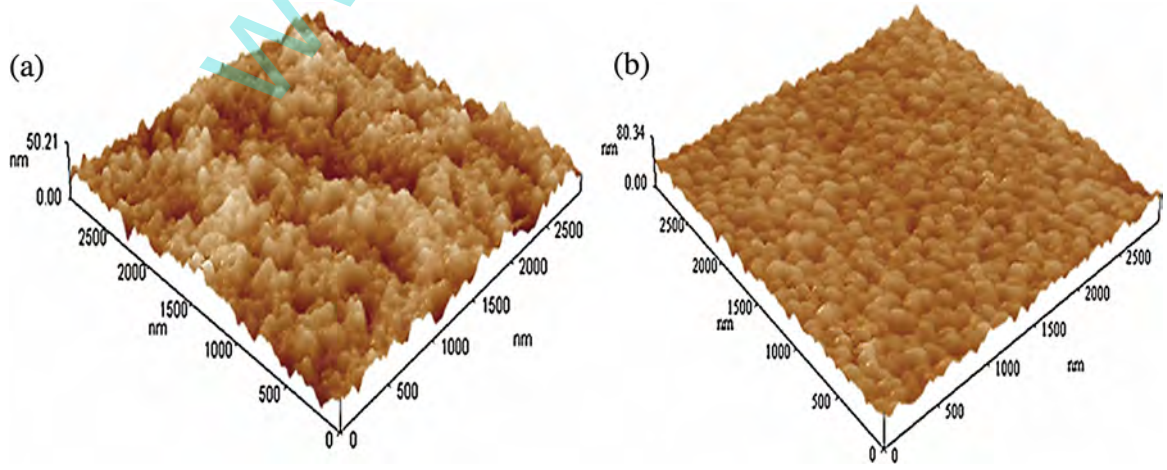

Fig. 5. AFM images of BZT–0.50BCT thin films (a) without LNO seed layer and (b) with LNO seed layer.

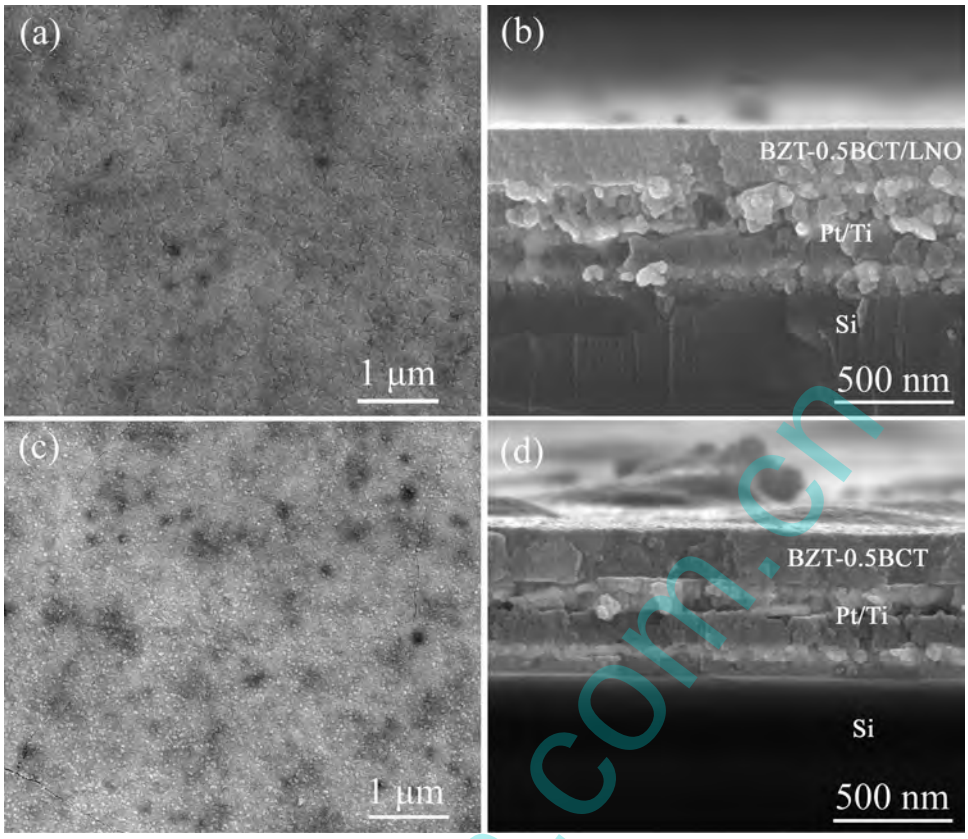

Fig. 6. SEM micrographs of BZT–0.50BCT thin film. (a) Surface micrograph of thin film with LNO seed layer, (b) cross-section micrograph of thin film with LNO seed layer, (c) surface micrograph of thin film without LNO seed layer, and (d) cross-section micrograph of thin film without LNO seed layer.

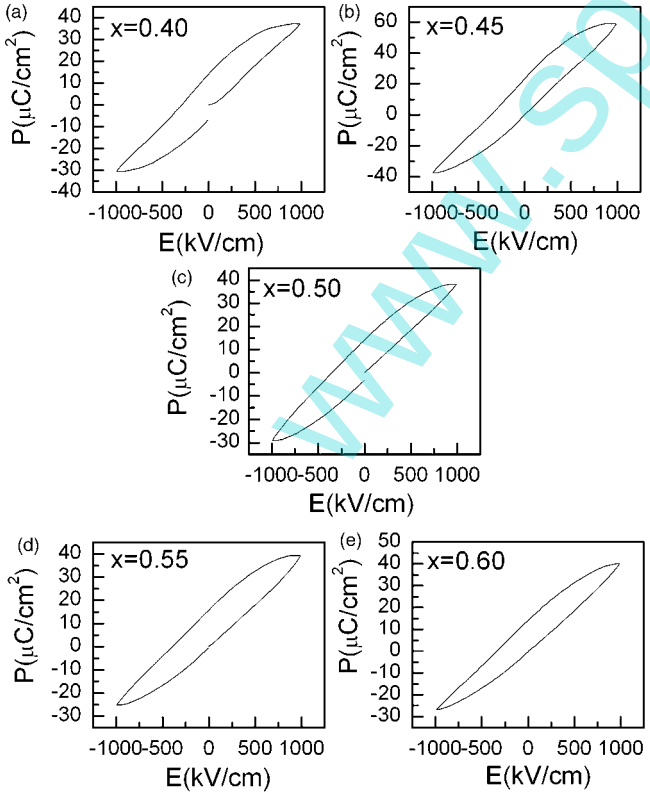

Fig. 7. P–E loops for BZT–*x*BCT/LNO thin film. (a) $x = 0.40$, (b) $x = 0.45$, (c) $x = 0.50$, (d) $x = 0.55$, and (e) $x = 0.60$.

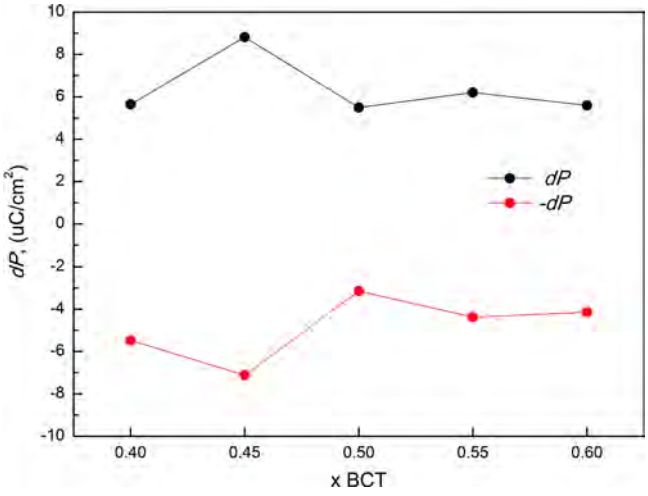

Fig. 8. $\pm dP$ response of BZT–*x*BCT/LNO thin films obtained from the PUND measurement.

the grain size of BZT–0.50BCT/LNO film is 140 nm which is bigger than the 130 nm for the film without LNO seed layer. In addition, LNO seed layer has an obvious influence on the surface roughness of the thin films, the roughness value is 5 nm for the film with LNO seed layer and 8 nm for the one without LNO seed layer, respectively. The SEM

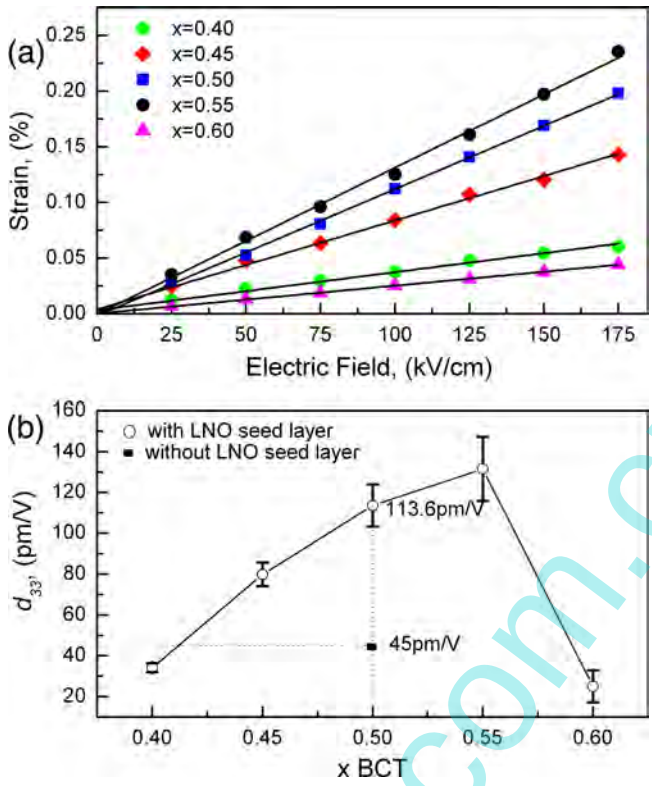

Fig. 9. Converse piezoelectric coefficients d_{33} of $(1-x)$BZT–xBCT/LNO thin films. (a) Linear fit of experimental data for $(1-x)$BZT–xBCT films, and (b) d_{33} values for different BCT content.

micrographs of the surface and cross-section of BZT–0.50BCT thin films were given in Fig. 6. The cross-section micrographs of SEM show that the thickness of the films is approximately 200 nm, there are not significant differences between the BZT–0.50BCT/LNO and BZT–0.50BCT thin films. However, the surface of BZT–0.50BCT thin film had some cracks as shown in surface micrograph of Fig. 6(c). To a great extent, the quality of the films was improved by the insertion of LNO seed layer. The LNO/Pt(1 1 1) substrate may provide nucleation sites and reduce the activation energy for the crystallization of (1 0 0)-oriented BZT–xBCT thin films, resulting in the formation of stoichiometric perovskite structure and better crystallinity. Zhai et al.[18] introduced LNO seed layer to enhance the electrical properties of BZT thin films and Li et al.[19] tried to obtain PMN-PT films of high quality on Si substrate buffered LNO seed layer.

The ferroelectric hysteresis loops provide another good evidence for the well-crystallized $(1-x)$BZT–xBCT/LNO thin films, as shown in Fig. 7. In order to avoid the apparent opening in the loops which could be due to dielectric loss, the 1000 kV/cm electric field was applied for the measurement. The shifts PE hysteresis loops in the electrical fields axes were noted, which may be caused by the presence of one polarization state over the other. The shifts in the polarization are due to the asymmetry of the top electrode and bottom electrode.[20] In order to eliminate the influence of leakage current to actual switchable component of the polarization in P(E) loops,[21] PUND (positive-up negative-down) measurement with a PA (pulse amplitude) of 10 V, PW (pulse width) = 1 ms and PD (pulse delay) = 10 ms was carried out using a Radiant Precision Workstation Ferroelectric Measurement System. Fig. 8 shows $\pm dP$ as a function of xBCT, and the peak dP value appears in the BZT–0.45BCT thin film which has the maximum orientation degree. It is worth noting that the variation of the true remanent polarization is strongly correlated with the (1 0 0)-orientation degree of thin films.

Fig. 9 shows the converse piezoelectric coefficients d_{33} of $(1-x)$BZT–xBCT/LNO thin films. The linear relationship between strain and applied voltage is shown in Fig. 9(a) and the slope, extracted from Fig. 9(a), represents the converse piezoelectric coefficient. As shown in Fig. 9(b), the maximum $d_{33} \sim 131.5$ pm/V appears at the composition of $x = 0.55$, higher than other compositions including $x = 0.50$ (113.6 pm/V) and 71.7 pm/V of the random oriented BZT–0.55BCT thin film[7] together with 80 pm/V and 100 ± 5 pm/V of the (1 1 1) oriented BZT–0.50BCT thin film.[8,9]

It is very reasonable that the compositions at both $x = 0.5$ and $x = 0.55$ around MPB have relatively higher d_{33} values. This may be attributed to the existence of the residual stress in the BZT–BCT thin films, which may lead to diffuse ferroelectric phase transition from R phase to T phase which broaden the MPB region. The diffuse phase transition caused by the distribution of stress was predicted by Wang.[22]

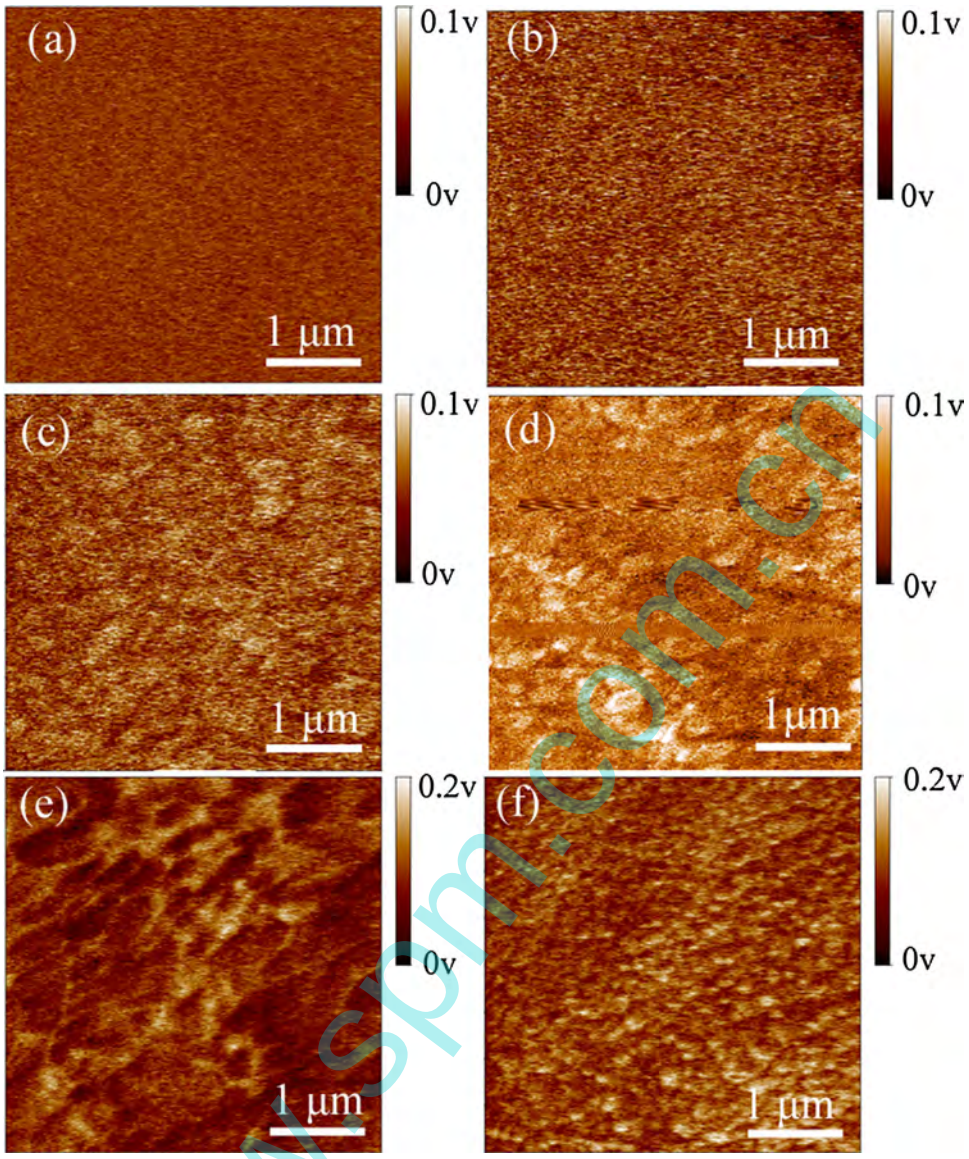

Fig. 10. PFM images of $(1-x)$BZT–xBCT thin film without LNO and with LNO seed layer. (a) $x = 0.50$ thin film without LNO seed layer, (b) $x = 0.40$, (c) $x = 0.45$, (d) $x = 0.50$, (e) $x = 0.55$, and (f) $x = 0.60$ thin films with LNO seed layer.

Additionally, as for the greatly enhanced piezoelectric properties compared with the reported d_{33} values[7–9] and our result of $d_{33} \sim 45$ pm/V for the BZT–0.50BCT film without LNO seed layer (see Fig. 9(b)), we attribute these results to the insertion of LNO seed layer, which influences the nucleation and growth dynamics of BZT–BCT films, and then improve the quality of the thin films with a more homogeneous grain size, smaller roughness, and some degree of (1 0 0) orientation. Moreover, the domain structure may play an important role on the piezoelectric property.[9,23] The PFM images were given in Fig. 10. In order to obtain the PFM images, the probing ac voltage (2 V, frequency 20 kHz) was applied between the conducting tip and bottom electrode of the thin films. The regions with a nonzero polarization could be visualized as areas with "black" or "white" contrast depending on the polarization orientation. There are obvious piezoelectric response at the compositions of $x = 0.50$ and $x = 0.55$ thin films as shown in Fig. 10(d) and (e) respectively. The weaker piezoelectric activity was observed in others composition thin films, especially the BZT–0.50BCT thin film without LNO seed layer as shown in Fig. 10(a).

Temperature dependence of dielectric properties for BZT–xBCT/LNO thin films at different frequencies were given in Fig. 11. The curve of $\varepsilon_r \sim T$ hints that the dielectric permittivity has a weak dependence temperature from 30 °C to 150 °C. According to the earlier research on BZT ceramics[24,25] and lead-free relaxor ferroelectrics,[26] a broad dielectric permittivity peak is achieved at the temperature T_m, which does not correspond to a phase transition from a paraelectric to a long-range-ordered ferroelectric state, instead, this phenomenon is related to relaxor dynamics. As x increases, it is apparent that the T_m of BZT–xBCT/LNO thin films shifts to a higher temperature from 65 °C to 120 °C. The T_m is about 115 °C at $x = 0.55$

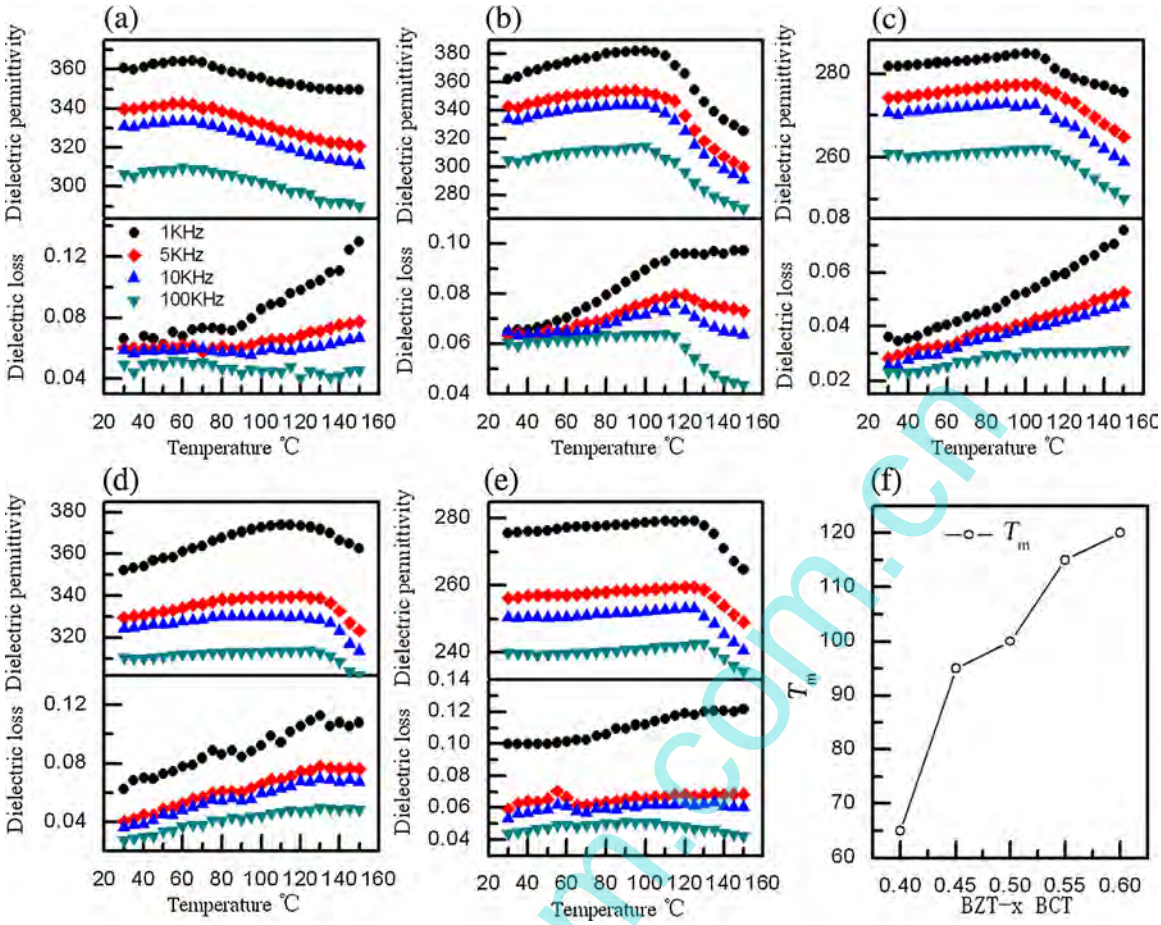

Fig. 11. Temperature dependence of the dielectric properties at different frequencies for BZT–xBCT/LNO thin films. (a) $x = 0.40$, (b) $x = 0.45$, (c) $x = 0.50$, (d) $x = 0.55$, (e) $x = 0.60$, and (f) T_m values for different BCT content obtained from the $\varepsilon_r \sim T$ at 1 kHz.

($d_{33} \sim 131.5$ pm/V). This change of T_m is properly attributed to the phase structure caused by the variation of composition in the films. The diffuse transition peaks at different frequencies are broader and shift toward higher temperatures slightly with increasing frequencies, which imply that the films exhibit relaxor behavior such as BZT thin film.[27,28]

4. Conclusion

In summary, the (1 0 0)-oriented $(1-x)$BZT–xBCT thin films were fabricated by sol–gel method, and an improvement in piezoelectric property was successfully achieved by the insertion of $LaNiO_3$ seed layer between the $(1-x)$BZT–xBCT thin films and substrates. Furthermore, the microstructure and electrical properties of the thin films were also studied. The films with LNO seed layer show promising ferroelectric, piezoelectric and dielectric properties. A notable piezoelectric constant of 0.45BZT–0.55BCT thin films reached 131.5 pm/V, which is higher than other films under the same system and close to the values of PZT films. These films are potential candidates for the lead-free piezoelectric applications.

Acknowledgment

The authors gratefully acknowledge support from Natural Science Foundation of China (Grant Nos. 11272102 and 51202049)

References

1. Ouyan J, Ramesh R, Roytburd AL. Theoretical investigation of the intrinsic piezoelectric properties for tetragonal $BaTiO_3$ epitaxial films. *Appl Surf Sci* 2006;**252**:3394–400.
2. Goh PC, Yao K, Chen Z. Lead-free piezoelectric thin films derived from chemical solution modified with stabilizing agents. *Appl Phys Lett* 2010;**97**:102901.
3. Rémondière F, Wu A, Vilarinho PM, Mercurio JP. Piezoforce microscopy study of lead-free perovskite $Na_{0.5}Bi_{0.5}TiO_3$thin films. *Appl Phys Lett* 2007;**90**:152905–11.
4. Son JY, Bang SH, Cho JH. Kelvin probe force microscopy study of $SrBi_2Ta_2O_9$ and $PbZr_{0.53}Ti_{0.47}O_3$ thin films for high-density nonvolatile storage devices. *Appl Phys Lett* 2003;**82**:3505.
5. Lahl U, Zeschmar-Lahl B. Risk based management of chemicals and products in a circular economy at a global scale (risk cycle), extended producer responsibility and EU legislation. *Environ Sci Eur* 2013;**25**:3.
6. Liu WF, Ren XB. Large piezoelectric effect in Pb-free ceramics. *Phys Rev Lett* 2009;**103**:257602.

7. Kang GQ, Yao K, John Wang. $(1-x)$–$x(Ba_{0.7}Ca_{0.3})TiO_3$ ferroelectric thin films prepared from chemical solutions. *J Am Ceram Soc* 2011: 1–6.
8. Piorra A, Petraru A, Kohlstedt H, Wuttig M, Quandt E. Piezoelectric properties of $0.5(Ba_{0.7}Ca_{0.3})TiO_3$–$0.5Ba(Zr_{0.2}Ti_{0.8})O_3$ ferroelectric lead-free laser deposited thin films. *J Appl Phys* 2011;**109**. AQ104101-1CAQ.
9. Luo BC, Wang DY, Duan MM, Li S. Orientation-dependent piezoelectric properties in lead-free epitaxial $0.5BaZr_{0.2}Ti_{0.8}O_3$–$0.5Ba_{0.7}Ca_{0.3}TiO_3$ thin films. *Appl Phys Lett* 2013;**103**:122903.
10. Zhu ZX, Ruangchalermwong C, Li JF. Thickness and Nb-doping effects on ferroelectric and piezoelectric properties of highly *a*-axis-oriented Nb-doped $Pb(Zr_{0.3}Ti_{0.7})O_3$ films. *J Appl Phys* 2008;**104**:054107.
11. Chen HD, Udayakumar KR, Gaskey CJ, Cross LE. Electrical properties' maxima in thin films of the lead zirconate–lead titanate solid solution system. *Appl Phys Lett* 1995;**67**:3411.
12. Li JF, Zhu ZX, Lai FP. Thickness-dependent phase transition and piezoelectric response in textured Nb-doped $Pb(Zr_{0.52}Ti_{0.48})O_3$ thin films. *J Phys Chem C* 2010;**114**:17796.
13. Zhao MH, Wang ZL, Mao Scott X. Piezoelectric characterization of individual zinc oxide nanobelt probed by piezoresponse force microscope. *Nano Lett* 2004;**4**(4):587.
14. Fei WD, Liu CQ, Ding MH, Li WL, Wang LD. Characterization of fiber texture by ω-scan X-ray diffraction. *Rev Sci Instrum* 2009;**80**:093903.
15. Li WL, Zhao Y, Fei WD, Chi QG, Song WT. Orientation degree dependence of magnetic properties of Co doped ZnO thin films by sol–gel process. *J Sol-Gel Sci Technol* 2010;**54**:335.
16. Yamada H, Suzuki T, Uchikoshi T, Hozumi M, Saito T, Sakka Y. Analysis of abnormal grain growth of oriented $LiCoO_2$ prepared by slip casting in a strong magnetic field. *J Eur Ceram Soc* 2013;**33**:3059–64.
17. Zhu XW, Sakka Y, Zhou Y, Hirao K, Itatani K. A strategy for fabricating textured silicon nitride with enhanced thermal conductivity. *J Eur Ceram Soc* 2014;**34**:2585–9.
18. Zhai JW, Gao Ch, Yao X, Xu ZK, Haydn Chen. Enhanced dielectric tenability properties of $Ba(Zr_xTi_{1-x})O_3$ thin films using seed layers on $Pt/Ti/SiO_2/Si$ substrates. *Ceram Int* 2008;**34**:905–10.
19. Li YW, Hu ZG, Yue FY, Yang GY, Shi WZ, Meng XJ, et al. Properties of highly (1 0 0) oriented $Pb(Mg_{1/3}Nb_{2/3})_3$–$PbTiO_3$ films on $LaNiO_3$ bottom electrodes. *Appl Phys Lett* 2007;**91**:232912.
20. Wang ZM, Zhao K, Guo XL, Sun W, Jiang HL, Han XQ, et al. Crystallization, phase evolution and ferroelectric properties of sol–gel-synthesized $Ba(Ti_{0.8}Zr_{0.2})O_3$–$x(Ba_{0.7}Ca_{0.3})TiO_3$ thin films. *J Mater Chem C* 2013;**1**:522–30.
21. Roy Chaudhuri A, Krupanidhi SB. Investigation of true remnant polarization response in heterostructured artificial biferroics. *Solid State Commun* 2010;**150**:660–2.
22. Lu XM, Zhu JZ, Liu ZG, Xu XS, Wang YN. Phase transition related stress in ferroelectric thin films. *Thin Solid Films* 2000;**375**:15–8.
23. Li W, Hao JG, Bai WF, Zhai JW. Orientation dependence of the dielectric and piezoelectric properties for the $Ba_{0.98}Ca_{0.02}Ti_{0.96}Sn_{0.04}O_3$ thin films. *J Sol-Gel Sci Technol* 2013;**66**:220–4.
24. Ciomaga CE, Buscaglia MT, Viviani M, Buscaglia V, Mitoseriu L, et al. Preparation and dielectric properties of $BaZr_{0.1}Ti_{0.9}O_3$ ceramics with different grain sizes. *Phase Transit* 2006;**79**:389–97.
25. Ciomaga CE, Calderone R, Buscaglia MT, Viviani M, Buscaglia V, Mitoseriu L, et al. Relaxor properties of $Ba(ZrTi)O_3$ ceramics. *J Optoelectron Adv Mater* 2006;**8**:944–8.
26. Shvartsman VV, Lupascu DC. Lead-free relaxor ferroelectrics. *J Am Ceram Soc* 2012;**95**(1):1–26.
27. Zhai JW, Yao X, Shen J, Zhang LY, Haydn Chen. Structural and dielectric properties of $Ba(Zr_xTi_{1-x})O_3$ thin films prepared by the sol–gel process. *J Phys D: Appl Phys* 2004;**37**:748–52.
28. Kleemann W, Miga S, Dec J, Zhai J. Crossover from ferroelectric to relaxor and cluster glass in $BaTi_{1-x}Zr_xO_3$ ($x = 0.25$–0.35) studied by non-linear permittivity. *Appl Phys Lett* 2013;**102**:232907.